Multipartite model of evaporative cooling in optical dipole traps

Matthew J. Williams and Chad Fertig

Phys. Rev. A **91**, 023432 — Published 27 February 2015

DOI: 10.1103/PhysRevA.91.023432

A multipartite model of evaporative cooling in optical dipole traps

Matthew J. Williams* and Chad Fertig
Department of Physics and Astronomy,
University of Georgia, Athens, Georgia 30602

We propose and study a new model of forced evaporation of atomic clouds in crossed-beam optical dipole traps that explicitly includes the growth of a population in the "wings" of the trap and its subsequent impact on dimple temperature and density. It has long been surmised that a large wing population is an impediment to the efficient production of Bose-Einstein condensates in crossed beam traps. Understanding the effect of the wings is particularly important for $\lambda = 1.06$ μm traps, for which a large ratio of Rayleigh range to beam waist results in wings that are large in volume and extend far from the dimple. Key ingredients to our model's realism are: (1) our explicit treatment of the non-thermal, time-dependent energy distribution of wing atoms in the full anharmonic potential; and (2) our accurate estimations of transition rates among dimple, wing, and free atom populations, obtained by Monte Carlo simulations of atomic trajectories. We apply our model to trap configurations in which neither, one, or both of the wing potentials are made unbound by applying a "tipping" gradient. We find that forced evaporation in a trap with two bound wing potentials produces a large wing population which can collisionally heat the dimple so strongly as to preclude reaching quantum degeneracy. Evaporation in a trap with one unbound wing, such as made by crossing one vertical and one horizontal beam, also leads to a persistent wing population which dramatically degrades the evaporation process. However, a trap with both wings tilted so as to be just unbound enjoys a nearly complete recovery of efficient evaporation. By introducing to our physical model an ad hoc, tunable escape channel for wing atoms, we study the effect of partially filled wings, finding that a wing population caused by single beam potentials can drastically slow down evaporative cooling and increase the sensitivity to choice of η.

PACS numbers: 37.10.De, 37.10.Vz, 34.10.+x

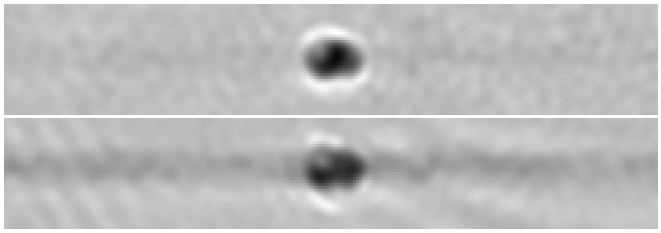

FIG. 1. Absorption images of a cloud of evaporatively cooled ^{87}Rb in the authors' apparatus, showing the formation of wings after 1 μs of forced evaporation at $\eta = 9.5$ in a λ=1.06 μm crossed beam dipole trap.

An atomic gas at temperature T, trapped by a conservative potential of depth U, will *evaporatively cool* to $T' < T$ as atoms stochastically promoted to the high-energy tail of the energy distribution escape the finite potential, the remaining atoms rethermalizing by collisions [1]. At each instant the evaporative cooling rate is proportional to $e^{-\eta}$: the fraction of atoms having an energy greater than the trap depth, where $\eta = U/k_BT$ [2] To maintain a high cooling rate as the temperature falls, the trap depth may be dynamically reduced so as to maintain a suitable value for η ("forced evaporation") [3]. A common method of producing such a dynamic trap is to spatially cross two off-resonance laser beams, of adjustable intensity, producing a deep and compact potential "dimple" at their intersection [4]. Evaporative cooling from optical dimple traps proceeds rapidly due to the large elastic scattering rates created by the high densities and tight confinement [5].

However, during forced evaporation in such a geometry, a large fraction of atoms that escape the dimple will flow into the long potential "wings" of each beam rather than escape to infinity, since the energy barrier for the former process is half that for the latter. It has been speculated that the formation of a large wing population may significantly impede the efficient evaporation of dipole trapped atomic clouds to quantum degeneracy. Barrett et al. [6] reported the observation of a large wing population during forced evaporation in a $\lambda = 1.06\mu$m trap, and speculated that the flow of atoms to the wings was responsible for their observed slow rate of increase of phase space density. In support of this hypothesis they performed a quasi-steady state calculation of the wing population for various trap depths, but did not explicitly model evaporation dynamics. Experimental steps taken to mitigate the "wings problem" have been previously reported in the literature. In [7] and [8], crossed beam traps were used in which a gradient was applied along one or both beams so as to "clear out" the wings. In [9] and [10], a strong potential gradient was applied perpendicular to the plane of the wings, forming a lip in the dimple over which evaporation could proceed without filling the wings. Curiously, [11] and [12] report successful evaporation of atomic clouds to quantum degeneracy without

* To whom correspondence should be addressed: mjw532@uga.edu

mention of any explicit measures taken to guard against the formation of a wing population.

A theory describing the effect of a wing population on evaporative cooling is lacking in the literature. Adams et al. briefly describe modeling of wing atoms trajectories in their seminal work on evaporating from a crossed beam dipole trap [4]. A detailed model of forced evaporative cooling in an isolated, isotropic, harmonic optical dimple was developed by Comparat et al. [13]; however, the model does not account for the growth of a wing population nor its back-action on the dimple. In experiments conducted in our lab, we observed rates of increase of phase space density during forced evaporation that were substantially less than predicted by a direct implementation of the model of [13]. We also observed the formation of a large, spatially extended wing population (Figure 1). These considerations motivated us to develop the model we report here.

I. A MULTIPARTITE MODEL OF EVAPORATION DYNAMICS IN CROSSED-BEAM OPTICAL TRAPS

In this section we lay out the framework of our multipartite model of evaporation in a crossed-beam potential, which explicitly includes the flow of atoms between the compact central dimple (at the intersection of the trapping beams) and the wing potentials (extending along the axis of each trapping beam). The essential components of our model are illustrated in Figure 2. We partition the total trapped population into two general groups: the "dimple" population of atoms confined to the crossing region of the two trapping beams, and the "wing" population of atoms whose orbits have turning points well outside the central dimple. A rigorous specification of these populations is given in Section I D. We use this model to investigate the nature and magnitude of the deleterious effect of the wings on the phase space density of the dimple atoms, and to investigate the efficacy of solutions to the wings problem based on the application of a "tilting" gradient to unbound one or both wing potentials.

In our model, we assume a thermal dimple population, and we approximate the dimple potential as simple harmonic when calculating elastic collision rates between dimple atoms. Because the volume of the wings is large, thermalizing collisions between wing atoms do not occur, even for large wing populations. Therefore we cannot and do not assume a thermal energy distribution for the wing atoms. It is essential to the realism of our model that we keep track of the time-dependent energy distribution of wing atoms. Our approach is to coarse-grain the continuous spectrum of wing atom energies into $M = 15$ bins. (We determine 15 bins to be sufficient by doubling the number of energy bins and repeating our calculations, finding no change in the results.) We model the evaporation dynamics by a system of $M + 2$ simultaneous, coupled, first-order differential equations for the number and energy of the dimple atoms and the number of atoms in each wing energy bin: N_d, E_d, and N_{w_i} $(i = 1, 2, \ldots M)$, respectively. We couple the dimple to the wings through the exchange of atoms at (the unequal) rates $\Gamma_{d\to w_i}$ and $\Gamma_{w_i\to d}$, and allow for the atoms to escape the trap at rates $\Gamma_{d\to f}$ and $\Gamma_{w_i\to f}$. As the trap depth is reduced during forced evaporation, the atoms in the wings can change from lower to higher energy bins at rates $\Gamma_{w_i\to w_{i+1}}$, which depend on i because the work done on the atoms by the time dependent potential is different for orbits of different total energy. We calculate all the rate coefficients relating to wing atoms by Monte Carlo simulations of atomic trajectories in the full 3D potential. For processes that involve only harmonically trapped dimple atoms we use expressions from Comparat et al. [13]; specifically, their expression for 2-body elastic scattering rates, loss and heating due to inelastic three body collisions, and heating due to the spontaneous scattering of trap photons, as well as approximate expressions for the temperature dependence of elastic collision cross sections and for the saturation of evaporation at high densities due to hydrodynamic effects.

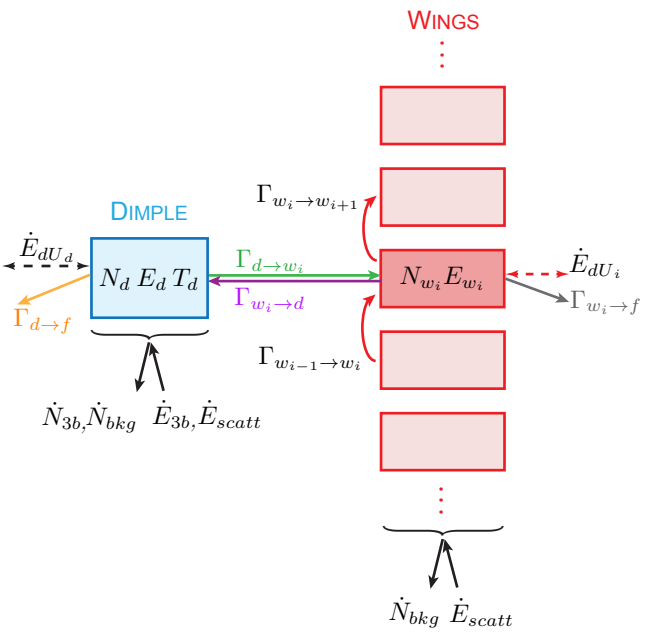

FIG. 2. (Color online) Block diagram of our multipartite model of a crossed-beam optical trap. Symbols are described in the text. Arrows depict rate constants for population changing processes. For clarity, only arrows connecting to the i$^{\text{th}}$ wing bin are shown. Dashed arrows depict mechanical work done on atoms due to changes to the trapping beam intensities. Rates shown as solid black arrows are taken from the model of Ref. [13]. Colors correspond to those of Figure 11.

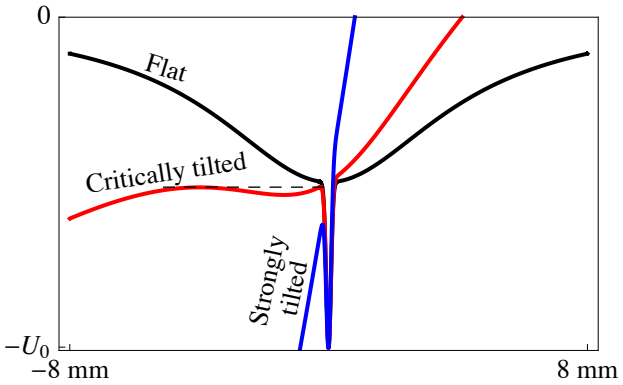

FIG. 3. (Color online) 1-D profiles through the total potential of a crossed beam dipole trap, along a single beam direction. In this work we simulate evaporation in flat traps (black) and critically tilted traps (red). Trap parameters are given in the text. We do not present results for a strongly tilted trap (blue), as we find it overkill as regards eliminating the wing population, while its extremely asymmetric evaporation lips make it difficult to compare with the flat trap.

A. Flat and tilted traps

We use our model to study evaporation from crossed-beam traps in which neither, one, or both wing potentials are unbounded in one direction ("flat," "singly tilted," and "doubly tilted" traps, respectively; see Figure 3). These traps can be made by superimposing a tilt gradient ∇U_{tilt} (e.g., using gravitational or magnetic fields) onto the crossed beam potential. (For examples, the singly tilted trap may be made from one horizontal and one vertical trapping beam; and a doubly tilted trap may be made by crossing the trapping beams at a shallow angle in a non-horizontal plane.) In this work we assume every atom experiences the same tilt gradient. When we require physical trap parameters for our calculations we use values taken from our experimental apparatus; specifically, we model ^{87} Rb atoms confined by two $\lambda = 1.06\mu$m beams crossing at their 76μm $1/e^2$ diameter waists at an angle of 14°. Figure 3 shows the total potential of this trap along the axis of one beam for no tilt, and for a critical tilt of $\nabla U_{tilt,crit} = 60U_0$ m^{-1}, at which the potential energy at apogee is just coincident with the energy lip to escape from the dimple to the wing—see dashed line on Figure 3. In this paper, we study traps that are either critically tilted. Calculations for strong tilts (beyond critical) are unenlightening as regards the "wings problem", as the evaporation physics becomes dominated by the distortion of dimple potential caused by the tipping gradient (see blue curve in Figure 3.)

B. Differential equations.

The processes shown in Figure 2 determine the time evolution of the dimple and wing atom numbers and energies. In this section we present the differential equations that describe the evaporation dynamics in our multipartite model.

1. *Evolution of the number in the dimple.*

In our model, the evolution of the number of atoms in the dimple population is given by:

$$\dot{N}_d = -\dot{N}_{d\to f} - \dot{N}_{d\to w} + \dot{N}_{w\to d} - \dot{N}_{bkg} - \dot{N}_{3b} \qquad (1)$$

Here, the rate at which the dimple population is depleted by elastic collisions among dimple atoms is $\dot{N}_{d\to f} = N_d\Gamma_{d\to f}$, where $\Gamma_{d\to f}$ is the rate (per dimple atom) at which (sufficiently energetic) dimple atoms escape the dimple to infinity, along any trajectory. Atoms with energy greater than $U_0/2$ are kicked into the wing part of the potential by elastic collisions with other dimple atoms at a rate $\dot{N}_{d\to w} = \sum_{i=1}^{M} N_d\Gamma_{d\to w_i}$, where $\Gamma_{d\to w_i}$ is the (per dimple atom) rate at which atoms are kicked to the i^{th} wing energy bin. Atoms in the wings are collisionally recaptured into the dimple population at the rate $\dot{N}_{w\to d} = \sum_{i=1}^{M} N_{w_i}\Gamma_{w_i\to d}$, where $\Gamma_{w_i\to d}$ is the rate (per wing atom in the i^{th} bin) at which wing atoms from the i^{th} energy bin are recaptured into the dimple population. The last 2 terms in Eq. (1) describe loss due to background gas collisions and three body recombination, and are taken directly from [13], to which we refer the reader for their detailed form.

2. *Evolution of the total energy in the dimple.*

In our model, the evolution of the total energy of the dimple atoms is given by:

$$\dot{E}_d = -\dot{E}_{d\to f} - \dot{E}_{d\to w} + \dot{E}_{w\to d} + \tfrac{1}{2}E_d\frac{\dot{U}_0}{U_0} + \dot{E}_{scatt,d} + \dot{E}_{3b,d} + \dot{E}_{bkg,d} \qquad (2)$$

Here, the dimple loses energy as atoms are ejected (to infinity) via elastic collisions at a rate $\dot{E}_{d\to f} = \varepsilon_{d\to f}\dot{N}_{d\to f}$, where $\varepsilon_{d\to f}$ is the average energy of such atoms. The dimple population also loses energy when dimple atoms are kicked into the wing population, via elastic collisions, at the rate $\dot{E}_{d\to w} = \sum_{i=1}^{M} N_d\varepsilon_{d\to w_i}\Gamma_{d\to w_i}$, where $\varepsilon_{d\to w_i}$ is the average energy of atoms kicked to the i^{th} bin at a (per dimple atom) rate of $\Gamma_{d\to w_i}$. The dimple gains energy when wing atoms are recaptured into the dimple, and their energy thermalized, at a rate $\dot{E}_{w\to d} = \sum_{i=1}^{M} N_{w_i}\varepsilon_{w_i}\Gamma_{w_i\to d}$, where ε_{w_i} is the energy of atoms in the i^{th} wing energy bin. The four remaining terms in Eq. 2 account for mechanical work done by the time-dependent trapping laser intensities, for the spontaneous scattering of trap laser photons, for three body recombination, and for background gas collisions, and come directly from [13], to which we again refer the reader for details.

3. Evolution of the total number and energy distribution of the wing population.

In our model, changes to the energy distribution and total energy of the wings population is reflected by changes to the populations N_{w_i}. The differential equation for the number N_{w_i} of wing atoms in the i^{th} energy bin is:

$$\begin{aligned}\dot{N}_{w_i} =&\dot{N}_{d\to w_i} + \dot{N}_{w_{i-1}\to w_i} - \dot{N}_{w_i\to w_{i+1}} - \dot{N}_{w_i\to d} \\ &- \dot{N}_{w_i\to f} - N_{w_i}\Gamma_{bkg}.\end{aligned} \tag{3}$$

Here, the rate at which dimple atoms are kicked by elastic collisions into the i^{th} wing energy bin is $\dot{N}_{d\to w_i} = N_d\Gamma_{d\to w_i}$. The rate at which wing atoms are promoted from one wing energy bin to the next, due to the reduction of trapping laser power during forced evaporation, is $\dot{N}_{w_i\to w_{i+1}} = N_{w_i}\Gamma_{w_i\to w_{i+1}}$. The rate at which atoms in the i^{th} energy bin are recapurted into the dimple population via elastic collisions with dimple atoms, is $\dot{N}_{w_i\to d} = N_{w_i}\Gamma_{w_i\to d}$. In a tipped trap, wing atoms in the i^{th} energy bin can escape the wing potential completely as they flow from the uphilll side to the downhill side. This occurs at a rate $\dot{N}_{w_i\to f} = N_{w_i}\Gamma_{w_i\to f}$. Note that although the direct escape channels for wing atoms, $\dot{N}_{w_i\to f}$, are zero in a flat trap, we find that very energetic wing atoms become dynamically decoupled from the dimple evaporation (see Section I D 2), justifying our decision to treat the term $\dot{N}_{w_M\to w_{M+1}}$ as a pseudo-escape-rate (i.e., we drop from further time evolution any atoms promoted to the "M+1" bin). We find that M=15 is sufficient to capture the relevant physics of the back-action of the wing atoms on the dimple, and that doubling he number of bins to 30 does not change our numerical results significantly. The last term in Eq. (3) is the loss rate due to collisions of wing atoms with background gas atoms. Finally, we comment that three body losses are negligible in the diffuse wings.

C. Calculation of transition rate constants

We next give equations for the rates $\Gamma_{\alpha\to\beta}$ of Eqs. (1-3).

$$\Gamma_{d\to f} = f^{(trap)}_{d\to f}\ \Gamma_{el}\ h(\langle n_{coll}\rangle) \tag{4}$$

$$\Gamma_{d\to w_i} = f^{(trap)}_{d\to w_i}\ \Gamma_{el}\ h(\langle n_{coll}\rangle), \tag{5}$$

where

$$trap \in \begin{cases} \text{flat} \\ \text{singly tilted} \\ \text{doubly tilted} \end{cases} \tag{6}$$

and

$$\Gamma_{w_i\to d} = \begin{cases} (1-p_{pass})2\frac{\omega_{w_i}}{2\pi} & \text{: flat or singly tilted} \quad (7a) \\ (1-p_{pass}) & \text{: doubly tilted} \quad (7b) \end{cases}$$

$$\Gamma_{w_i\to f} = \begin{cases} 0 \text{ for } i < M & \text{: flat or singly tilted} \quad (8a) \\ p_{pass}2\frac{\omega_{w_i}}{2\pi} & \text{: doubly tilted} \quad (8b) \end{cases}$$

$$\Gamma_{w_i\to w_{i+1}} = \langle 1/t_{res,i}\rangle$$

In Equations (4) and (5) Γ_{el} is the two-body elastic collision rate and $h(\langle n_{coll}\rangle)$ is an empirical function which throttles evaporation in clouds close to the hydrodynamic regime (see [13]). Dimple atoms kicked (via elastic collisions with other dimple atoms) to energies greater than $U_0/2$ may, with probabilities $f^{(trap)}_{d\to w_i}$ and $f^{(trap)}_{d\to f}$, enter the i^{th} wing bin, or leave the trap entirely, respectively. In Equation (7), $\Gamma_{w_i\to d}$ is the rate at which the dimple recaptures wing atoms from the i^{th} wing energy bin. We assume that single collision with a dimple atom leads to the recapture and thermalization of the wing atom into the dimple population. The probability for a single wing atom to collide with any dimple atom in one transit through the dimple cloud of thermal radius r_{th} is $p_{coll} = \frac{\sigma}{4\pi r^2_{th}}$ [16], where σ is the two-body elastic scattering cross-section. Using this expression we derive p_{pass}, the probability for a wing atom to pass once through the entire dimple cloud without colliding: $p_{pass} = (1-p_{coll})^{N_d}$. ω_{w_i} is the longitudinal angular frequency for a wing atom of energy ε_i. $2\ \frac{\omega_{w_i}}{2\pi}$ is the attempt rate for wing atoms of energy ε_i to collide with a dimple atom. The details of the calculation of ω_{w_i} are given in Section I D.

In a doubly tilted trap, wing atoms with initially uphill trajectories are turned by the tilt gradient, pass once through the dimple, and—if they do not collide with a dimple atom—escape to infinity on the downhill side. Atoms with initially downhill trajectories are counted as prompt escapes, and are not included in the wing population. In a flat trap, a wing population may extend along both trapping beams, and all wing atoms may make multiple passes through the dimple. In a singly tilted trap the situation is more complicated, in that there exists a wing population along one beam with the properties of a tilted trap, and a wing population along the other beam with properties of a flat trap. This raises the question whether atoms in the flat-beam wing may not, in the course of crossing through the dimple, *transfer* into the tilted wing and escape the trap. In fact, we find, by direct Monte Carlo simulation of $> 10^4$ different trajectories, vanishing probability for this escape process, even for tilts as large as $100(\Delta U)_{tilt,crit}$. In other words, bound wing trajectories scatter off the dimple potential into other trajectories bound to the same wing with nearly unit probability. (We estimate the effect of wing-to-wing transfers due to glancing collisions between wing and dimple atoms to be a next-to-leading order correction to our model.)

D. Determining model parameters through Monte Carlo simulations of atom trajectories

We use Monte Carlo techniques to numerically estimate the 62 model parameters $f_{d\to f}$, $f_{d\to w_i}$, ω_{w_i}, $t_{res,i}$ $\varepsilon_{d\to f}$, and $\varepsilon_{d\to w_i}$, each of which are functions of both the absolute trap depth and its time derivative. Additionally, each quantity also depends on the details of the trap geometry, and so must be recomputed for each of the trap types enumerated in Eq. (6).

1. *Trap specific energy dependencies of dimple-to-wing and dimple-to-free transitions.*

An atom in the dimple population (viz., having an orbit which, if unaltered, remains in the dimple) is subject to elastic collisions with another dimple atoms that may, with probability $p_{d\to\alpha}$, kick it into a wing ($\alpha = w$) or free ($\alpha = f$) trajectory. The fraction of all dimple atoms kicked into such trajectories is found by a Boltzmann weighted average of $p_{d\to\alpha}$ with respect to energy:

$$f_{d\to\alpha} = 2\pi^{-1/2}\,(k_B T)^{-3/2}\int_0^\infty p_{d\to\alpha}^{(trap)}\,\sqrt{E}\,e^{-E/k_B T}dE. \tag{9}$$

The average energy of the ejected atoms is given by:

$$\varepsilon_{d\to\alpha} = \frac{\int_0^\infty E\,p_{d\to\alpha}^{(trap)}\,\sqrt{E}\,e^{-E/k_B T}dE}{\int_0^\infty p_{d\to\alpha}^{(trap)}\,\sqrt{E}\,e^{-E/k_B T}dE}, \tag{10}$$

We conduct Monte Carlo simulations to estimate the $p_{\alpha\to\beta}^{(trap)}$, the probabilities for a various outcomes of a dimple atom elastically colliding with another dimple atom. The possible outcomes are that the first atom could be launched on (1) another dimple-bound trajectory (undergoes a dimple→dimple transition), (2) a wing-bound trajectory (undergoes a dimple→wing transition), or (3) is kicked out of the trap (undergoes a dimple→free transition). To estimate these probabilities, we numerically calculate and categorize classical trajectories in the full 3D potential. The trajectories are invariant under scaling that preserves the ratio E/U_0; however they must be recomputed for each value of $\nabla U_{tilt}/U_0$. Specifically, in each run we compute trajectories for 2000 atoms launched with common energy E from the center of the dimple, but in random directions. This is repeated for each of the trap types of Eq. (6), and for many energies E chosen on a mesh from $E = 0$ to $2U_0$.

The trajectories are categorized as either (1) a dimple-bound trajectory, (2) a wing-bound trajectory, or (3) an unbound (free) trajectory, according to the following rubric: Any trajectory that ever accelerates away from the trap center cannot return, and is therefore classified as free. Any trajectory that exhibits a turning point in its radial coordinate is certainly bound. If a bound trajectory has a turning point inside an ellipsoidal volume having minor radius extending to the $0.99U_0$ contour in

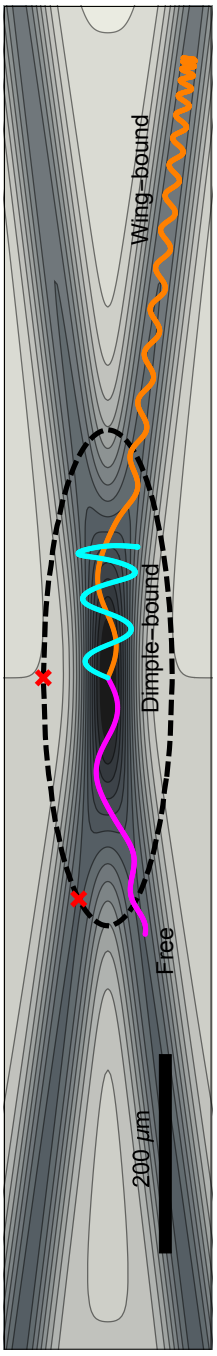

FIG. 4. (Color online) Example atomic trajectories in the total potential of a doubly critically tilted crossed-beam dipole trap. The "downhill" (i.e., unbounded) wings are shown on the bottom of the plot. Red "X's" locate the positions in the potential which fix the location of the fiducial ellipsoid (black dashed curve) that demarcates the dimple volume. The three example atoms are launched in different directions from the center of the trap, each with energy equal to $0.6U_0$. The cyan curve is a "dimple-bound" trajectory because it has a turning point inside the ellipsoid. The orange curve is a "wing-bound" trajectory because it has a turning point outside the ellipsoid. The magenta curve is a "free" trajectory because it is accelerating away from the trap center and cannot return.

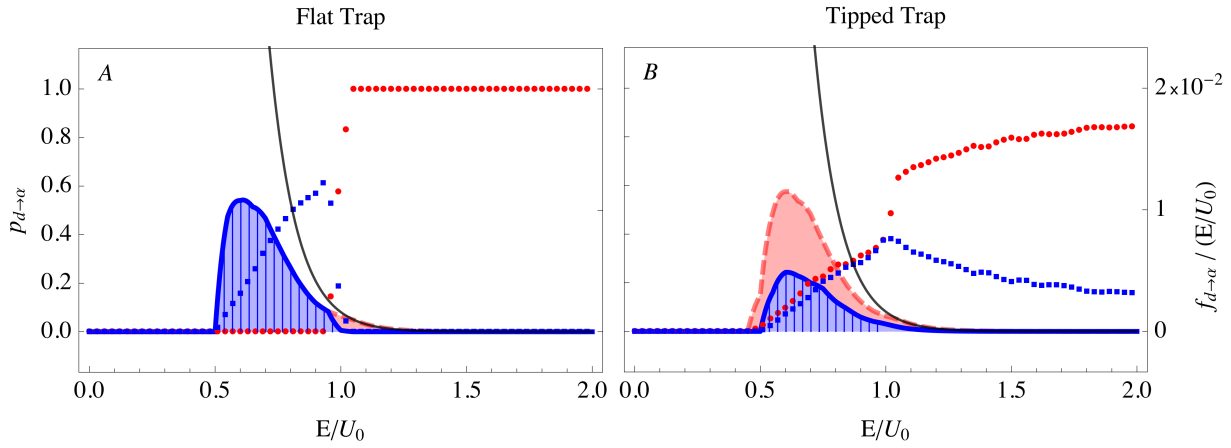

FIG. 5. (Color online) Monte Carlo calculations of dimple→wing ($d \to w$) and dimple→free ($d \to$f) transition rates in flat traps (panel A) and tipped traps (panel B). Points are probability densities versus energy for the outcome of a collision between dimple atoms to kick one colliding partner into a wing-bound trajectory ($\alpha = w$, blue squares) or to a free trajectory ($\alpha = f$, red points). The probability densities are calculated by the Monte Carlo simulation described in section I D, and are referred to the left axis. The solid curves show the transition probabilities (points) convolved with the Boltzmann distribution (thin black line) for $\eta = 10$ traps, and are referred to the right axis. (Note that the solid curves must be recomputed for every η.) The shaded area is the total probability for collisions between dimple atoms to eject a dimple atom from the trap entirely (area under the red dashed curve), or into the the wing population (area under the blue curve); for the latter, each vertical bar represents the probability for an individual wing energy bin. These results show that, for this flat trap, 94% thermalizing collisions which kick dimple atoms out of the dimple send them into the wings, rather than ejecting them from the trap entirely. In stark contrast, for the critically tipped trap, 60% of the atoms kicked from the dimple by elastic collision with other dimple atoms promptly escape to infinity through the downhill wing.

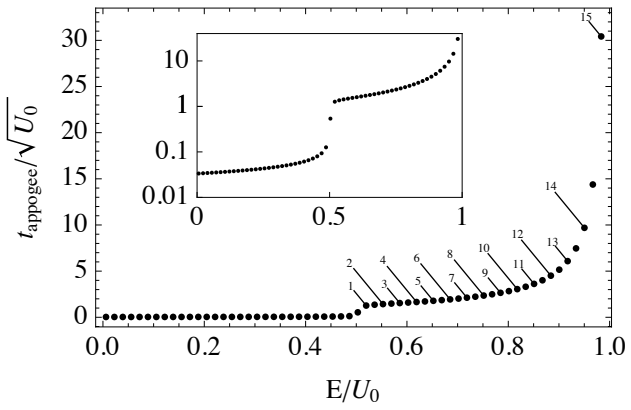

FIG. 6. Scaled t_{apogee} versus scaled energy for dimple atoms launched on new trajectories by collisions with other dimple atoms, in a flat trap. Orbital energies corresponding to the bin energies ε_i (i=1..15) are indicated. For $E/U_0 > 0.5$, t_{apogee} increases dramatically because atoms have enough energy to enter the wing part of the trapping potential. The large t_{apogee} for wing atoms occupying the last few energy bins greatly suppresses their backaction on the dimple. Note that these results are specific to given trap parameters (beam waist, crossing angle, etc.). However, as remarked in the text, the scaled t_{apogee} is independent of trap depth, and so a single set of calculations is valid for the entire forced evaporation sequence. Inset: same data, plotted on a semi-log scale.

the tight direction of the dimple potential and major radius extending to the $0.99(U_0/2)$ contour in the loose direction of the dimple potential (dashed curve, Figure 4), the trajectory is classified as dimple-bound; otherwise it is wing-bound. To avoid having to follow exotic orbits for inconveniently long simulation times, we apply two additional criteria to classify some trajectories as "practically" free: if the trajectory reaches more than 2 cm from the trap center, or if it reaches a position where the optical potential is less than $10^{-3}U_0$, we terminate the calculation and classify the trajectory as free. Examples of some trajectories are shown in Figure 4. By tallying the destinies of the computed trajectories, we estimate the transition probabilities $p_{d\to\alpha}$, and the energy-weighted transition fractions $f_{d\to\alpha}$, for many values of E/U_0, for both flat and tipped traps; these are displayed graphically in Figure 5.

2. *Trap-type-specific energy-dependencies of the wing→dimple recapture rate.*

To uncover the backaction of the wing atoms on the dimple evaporation dynamics, we must compute the wing+dimple collision rate, a quantity that depends both on the frequency with which wing atoms cross the dimple, as well as the per-crossing collision probability. The orbital oscillation period of an atom in the crossed beam dipole trap is a strong function of energy due to the extreme anharmonicity of the full potential. We use numer-

ical methods to calculate the longitudinal wing frequency ω_{w_i} for atoms having fractional energy $0 < E_{w_i}/U_0 < 1$. Specifically, we numerically integrate the motion of atoms launched from the center of the dimple of a (static) trap until they reach their turning point at time t_{apogee}. This time is used to define a characteristic angular frequency of the orbits: $\omega_{w_i} = 2\pi/4t_{apogee}$. Of course, during forced evaporation many wing atoms do not complete one orbit before the trap potential changes significantly. However, we make the reasonable assumption that *at each instant* there is a sufficiently large number of wing atoms in each wing energy bin, uniformly distributed in their orbital phases, such that the average rate at which wing atoms of energy E_{wi} cross the dimple is well approximated by $2\pi\omega_{w_i}$. As the trap depth U_0 decreases during forced evaporation, ω_{w_i} scales $\propto U_0^{-1/2}$ (in complete agreement with the harmonic case) so that one set of numerical calculations can be used over the entire evaporation sequence. In Figure 6 we plot a scaled time-to-apogee: $t_{apogee}/\sqrt{U_0}$. The plot is valid at all times during evaporation as long as a fixed (relative) tilt gradient is maintained, as discussed in Section I A.

3. Bin Residency Time

During forced evaporation, the trap depth is dynamically reduced as the cloud cools. Generally, any change in the optical potential results in mechanical work being done on the trapped atomic gas. This "optical work" plays an essential role in the evaporation dynamics in a dimple trap with a large wing population. Unfortunately, three facts conspire to complicate the modeling of optical work: (1) the wing population is non-thermal; (2) the wing potential is highly anisotropic; and (3) significant changes to the trap potential take place on times scales much shorter than wing atom oscillation periods.

In our model, we account for changes to the wing population energy distribution due to optical work by introducing population transition rates between adjacent wing energy bins. Under the reasonable assumption that during forced evaporation the trap laser intensity is decreased monotonically, we find that these transitions only occur in one direction: from lower to higher energy bins. The inverse of these wing-to-wing rates are the "bin residency times" $t_{res,i}$: the time a wing atom dwells in the i^{th} bin. During the dynamics of forced evaporation, the bin residency time is a complicated function of both the absolute trap depth U_0 and the ramping rate $\dot{U}_0/U_0$. Fortunately, we find that there is strong correlation between these two quantities for a wide variety of realistic evaporation ramp sequences. Thus we find that we can restrict our computation of bin residency times to a small slice of the full space of $U_0 \otimes (\dot{U}_0/U_0)$, thereby greatly reducing computational burden of this step.

We compute the set of residency times $t_{res,i}$ for hundreds of different values of $\dot{U}_0/U_0$, chosen on a logarithmic mesh on the range 0 to 10^3, which occur over the course of a hypothetical, realistic evaporation sequence (Figure 7). At each mesh point we perform a Monte Carlo simulation of 300 wing atoms launched from the center of the trap with an initial energy slightly less than the lower limit of the lowest ($i = 1$) energy bin, and with random orbital phases. We numerically integrate each atom's trajectory as the trapping laser power is reduced. Using these trajectories we calculate (from kinematics) the time during which each atom's energy falls within the range associated with each wing energy bin. Figures 7B-D show scatter plots of the bin residency times for each of the 300 atoms at three representative mesh points of the evaporation ramp of Figure 7A. We take the mean values of the distributions in each bin as the t_{res_i} of Eq. 9. This database of wing bin residency times is the final ingredient to our realistic model of forced evaporation in a crossed-beam optical dipole trap.

II. EVAPORATION CALCULATIONS

In the second part of this paper we use our model to study forced evaporation in optical dipole traps. While our model equations are general, the model parameters must be re-computed (c.f., Section I D) for different initial conditions, trap geometry, and evaporation sequences. This is not a weakness of our model, but rather a reflection of the highly contingent evolution of non-thermal wing atoms moving in an anharmonic trap that is undergoing non-adiabatic changes in depth. The particular trap parameters for which we solve our model were given in Section II C; with the additional specification of the following initial conditions: we start with 6×10^6 atoms at a temperature of $200\mu K$ in a $2000\mu K$ deep trap. Using these initial conditions we numerically solve [17] our model Equations (2-4) for 100 s of model time or until the phase space density ρ reaches the condensation threshold of $\rho = 2.6$. We perform forced evaporation by reducing the optical power so as to maintain a constant value of $\eta = U_0/k_BT$. In tilted traps, the tilt ratio $\nabla U_{tilt}/U_0$ is held constant at the critical value (c.f. Section I A). To simplify the interpretation of our results, we set the background gas collision rate to zero (unless otherwise specifically stated), and we use the time-to-condensation t_c as the metric by which to compare evaporation strategies.

A. Forced evaporation in a flat trap with wings.

In Figure 8 we present the first set of results from our modeling of forced evaporation in a flat trap. We plot both t_c and the number of dimple atoms remaining at condensation, N_c, over a range of evaporation sequences characterized by different (but constant) values of η. We observe that t_c exhibits a broad minimum from $8 < \eta < 9$, then jumps dramatically upwards at $\eta \approx 9.4$. Our results also show that N_c increases to its maximum value

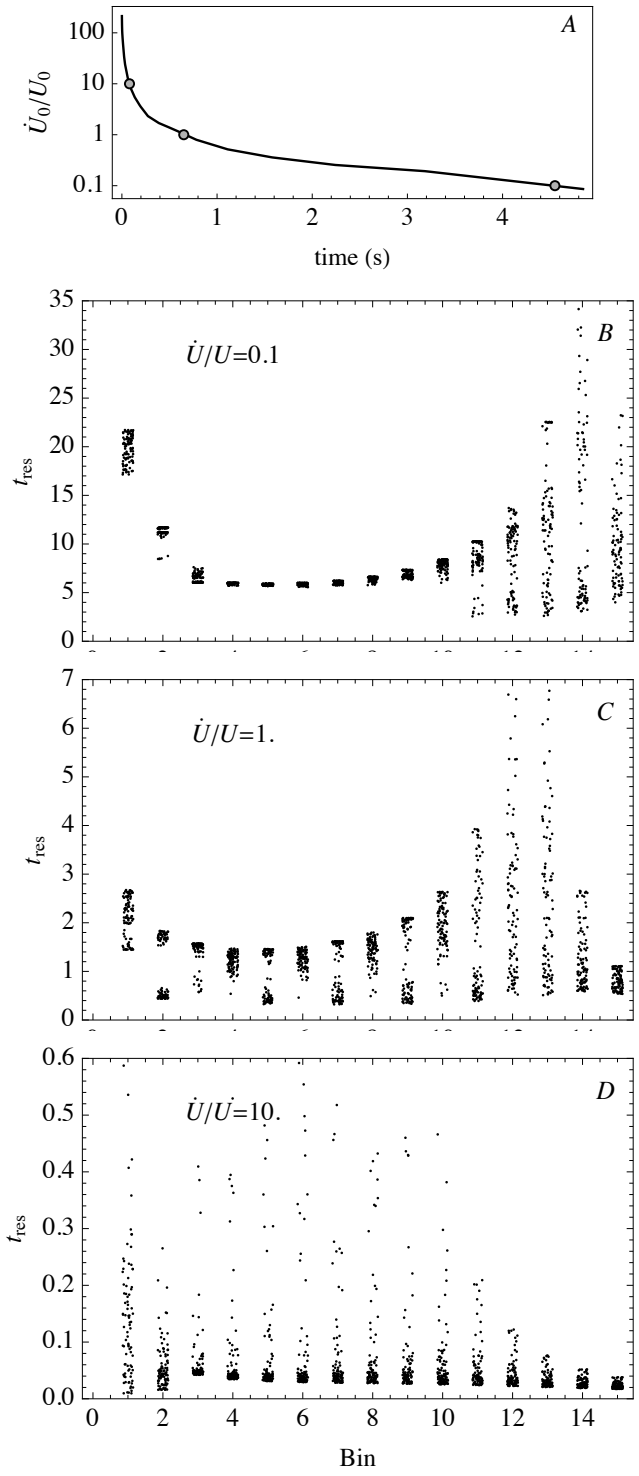

FIG. 7. Monte Carlo calculations of wing energy bin residency times $t_{res,i}$. Panel A: $\dot{U}_0/U_0$ versus time for a hypothetical forced evaporation sequence in a flat trap. In Panels B–D, each point corresponds to one atom spending some amount of time in the energy range corresponding to a particular wing energy bin, at three representative epochs in the evaporation sequence of (circled points in Panel A). The distribution of $t_{res,i}$ in each energy bin reflects both the non-adiabaticity and dependence on initial conditions. To fully implement our model, hundreds of these data sets are generated for $\dot{U}_0/U_0$ between .01 and 1000.

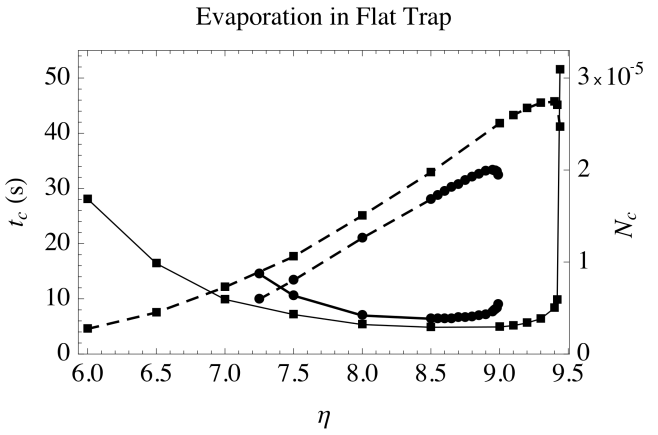

FIG. 8. Optimizing forced evaporation at constant η in a flat trap. Shown are the time to condensation t_c (solid symbols, left axis), and number in the dimple at t_c (open symbols, right axis), for η between 6 and 9.5. For a sample in which background lifetime is ignored ($\tau = \infty$) evaporation at $\eta > 9.5$ does not yield a condensate in less than 100s. Circles represent calculations of forced evaporation for a somewhat more realistic case where the background gas collision rate corresponds to a background collision limited lifetime of $\tau =$ 60s. Lines are guides to the eye.

at $\eta = 9.4$, after which it precipitously declines. The square symbols of Figure 8 are calculated for the case when background gas collisions are negligible. Using a finite background lifetime of $\tau_{bg} = 60$s (circle symbols of Figure 8), the time to condensate is longer, and the number of atoms in the dimple at condensation is less, for η near its optimal value. More striking, however, is the appearance of upper and lower limits for η, beyond which it is no longer possible to achieve condensation.

To investigate the nature of the divergence of t_c at $\eta = 9.4$, we plot in Figure 9 the phase space density of the dimple versus time for η at slightly below and slightly above this critical value. The curves are similar during the first 4 seconds of evaporation. The curve for $\eta = 9.4$ is clearly flattening as the condensation threshold is reached approximately 10 seconds into the ramp. The curve for $\eta = 9.5$ exhibits a sub-threshold maximum around $t = 10$s, followed by a period of slow decline over the next 20 seconds, followed by a period of even slower growth. If the background lifetime permits, the sample will still condense (at a time beyond 50s); if background losses are non-negligible the dimple may be totally depleted of atoms before condensation can occur. Figure 9 is an example of the precipitous drop in evaporative cooling performance which can be caused by the influence of energetic atoms from the wing population.

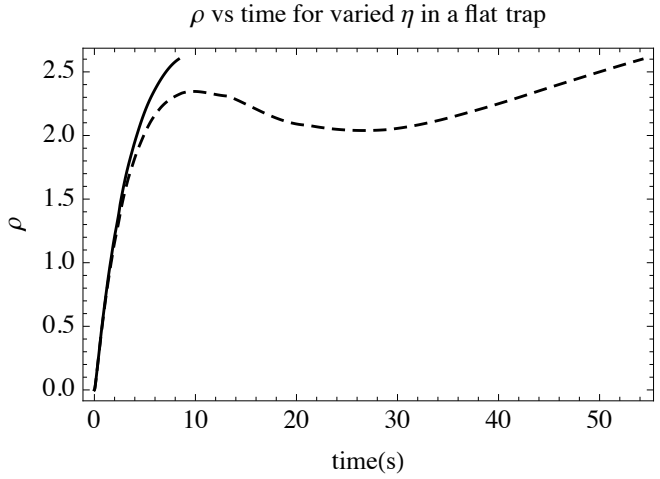

FIG. 9. Phase space density vs time for evaporation in a flat trap at η of 9.4 (solid line) and 9.5 (dashed line). The curve for $\eta = 9.5$ displays a local maximum just below threshold, and does not recover forward progress until after ∼30 seconds of evaporation.

B. Comparing forced evaporation in flat, singly tipped and doubly tipped traps.

In this section we use our model to compare evaporation in flat, singly-tipped, and doubly-tipped traps, and ascertain the impact of the wing population on the evaporation of the dimple in each configuration. The main finding of this section is that, by applying a tipping gradient so as to unbound one or both wings, we are able to decrease the time to condensation, and by reducing or eliminating the wing population.

In Figure 10 we show the time-to-condensation t_c for various constant-η evaporation sequences in flat, singly tipped, and doubly tipped traps; the blue circles of Figure 10 are the same data as the squares of Figure 8, reproduced to facilitate comparison. For our trap parameters and initial conditions, we find that constant-η forced evaporation in a flat trap is optimal at $\eta_{opt} = 8.5$, reaching condensation after $t_c = 4.8$ s of evaporation with $N_c = 2\times10^5$ atoms remaining in the dimple. Evaporation in a singly-tipped trap is optimized at a slightly higher $\eta_{opt} = 9$, reaching condensation faster ($t_c = 3.1$s) and with more dimple atoms remaining ($N_c = 2.9 \times 10^5$). In a doubly-tipped trap, evaporation is optimized at $\eta_{opt} = 11$, and condensation at reached in less than half the time for the flat trap ($t_c = 1.9$s), and with twice the final number of dimple atoms ($N_c = 4 \times 10^5$). Thus, our calculations suggest that each trap is capable of producing a sizable condensate in a reasonable time, with significantly different η_{opt} in each case. The most striking aspect of Figure 10 is how much less forgiving the flat trap is to slight inaccuracies in the η of the evaporation sequence, as compared to either the singly- or doubly-tipped traps. These results recommend against the flat trap for the reliable production of condensates, given the inevitable variation and inaccuracies in the execution of pre-programmed evaporation sequences.

In Figure 11 we show how the energy flow rate terms of Equation 2 change over the course of evaporation, for the three types of traps. The evaporation sequence in each trap is a constant-η ramp at the optimal values found in the previous section. In the flat trap (panels A1 and A2), we find that a large cloud of energetic atoms builds up in the wings. These energetic atoms heat the dimple (panel A1, red curve), by recapture and thermalization, at a rate that eventually exceeds the rate at which the dimple cools by direct evaporation (panel A1, gold curve). For the doubly-tipped trap (panels C1 and C2), no large persistent wing population develops, and the dimple heating rate due to the recapture of wing atoms is always lower than the rate at which the dimple evaporates. The singly-tipped case (panels B1 an B2) qualitatively resembles that of the flat-trap. However, we forego a detailed comparison of the energy flow rates between the various traps because the effective evaporation energy lip is significantly different in each case, due to different η_{opt}. In section III we will introduce a variation to our model to help to isolate the effect of the wing population on evaporation.

C. Variation of trap conditions

The results presented thus far were obtained for simulations made with the trap parameters and initial conditions matching those of our particular experimental realization. In a step towards generalization, we here repeat the calculations of Figure 10 for small, but significant, variations in the beam waist, initial number and initial temperature. Figure 12 shows the results of these further simulations. In Figure 12A we show t_c versus the evaporation η for flat and tipped traps made with lasers focused to waists smaller and larger than those in our experimental system. With the other experimental parameters and initial conditions held constant, these three traps have (different) initial phase space densities of 3.9×10^{-4} (42μm waist radius), 5.3×10^{-4} (38μm waist radius) and 7.4×10^{-4} (34μm waist radius). This variation of the beam waist radius by $\pm10\%$ makes a $\sim 3\times$ change in the time to condensation for evaporation in a flat trap (panel A, blue curves), but the critical value of η (above which condensation does not occur) stays at 9.5. For the tipped-trap case (panel A, red curves) we see a weaker effect of changing the waist size. Finally, we see that the wings have less of a harmful impact on the tighter-waist traps, as revealed in the diminishing difference between flat and tipped (i.e., blue and red curves) as the waist is tightened.

In Figure 12B, we present calculations where we vary the initial temperature of the trapped atoms; specifically, we calculate for $T_0 = 250\mu K$ ($\rho = 2.7\times10^{-4}$), $200\mu K$ ($\rho = 5.3\times10^{-4}$), and $150\mu K$ ($\rho = 1.3\times10^{-3}$). A 25% variation in temperature yields a $\sim 3\times$ change in the

time to condensation for evaporation in a flat trap, and has a larger effect on the flat trap as compared to the tipped trap. Also, we find that the critical value of η decreases for initially hotter clouds. Finally, we see that the wings have less of a harmful impact on initially colder clouds, as revealed in the diminishing difference between flat and tipped (i.e., blue and red curves) as the initial temperature is reduced.

In Figure 12C, we show results for different initial numbers of atoms such that the associated initial phase space densities are exactly those encountered in the temperature study. Specifically, we chose $N_0 = 3 \times 10^6$ atoms ($\rho = 2.7 \times 10^{-4}$), 6×10^6 atoms ($\rho = 5.3 \times 10^{-4}$), and 1.4×10^7 ($\rho = 1.3 \times 10^{-3}$). The time to condensation was far more sensitive to changes in initial number than initial temperature (for the same initial ρ), particularly in the case of the flat trap. In fact, the lowest atom number case did not produce a condensate in 100 seconds of evaporation, and so the curve does not appear on the figure. Over the range of parameters we explored, we find that, for a given initial phase space density, it is better to start evaporation with more, hotter atoms than fewer, colder atoms, but that the difference is far more significant in the flat trap, evidently because of the deleterious impact of the wing population.

By studying the behavior of our model under small but significant alternations to our base set of experimental parameters, we find two general features emerge: 1) flat traps generally suffer from a persistent wing population which interfere with efficient evaporation, and 2) doubly-tipped traps always produce a larger condensate, more quickly, and over a wider range of constant η evaporation ramps, than flat traps.

III. A TOY MODEL WITH TUNABLE WING-TO-DIMPLE FRACTION

The three physically realizable trap potentials we studied in Section II—flat, singly tilted, and doubly tilted—differed both in the how atoms flowed from the dimple to the wings, and in how the wing population evolved in number and temperature. To better understand the specific dependence of evaporation dynamics on wing population, we augment our flat trap model with an additional, fictitious loss rate for wing atoms, permitting us to study traps with steady-state wing populations that deviate from the "on shell" solutions studied so far. This is accomplished by modifying Eq (8a), for the case of the flat trap, to have the form

$$\Gamma_{w_i \to f} = \kappa \, \Gamma_{d \to w_i} \tag{8a$'$}$$

which reduces to (8a) for $\kappa = 0$. When $\kappa = 1$, a wing population does not form during evaporation. By solving our model for intermediate values of $(0 < \kappa < 1)$, we investigate how the number of wing atoms influences the production of a condensate. In this interest, we set $\Gamma_{bkg} = \Gamma_{spon} = \Gamma_{3b} = 0$, which highlights the effect of the wings on the dimple.

In Figure 13 A we show the time to condensation t_c vs η for $\kappa = (0, 0.2, 0.4, 0.6, 0.8, 1)$. We find that t_c increases dramatically with increasing fractional wing population for a evaporation at fixed η, and furthermore that η_{opt} increases with increasing wing population. In Figure 13B we show the time-dependence of the wing populations for those same six values of kappa, for evaporation conducted at η_{opt}.

IV. CONCLUSION

In this work we have applied a novel, multipartite model of forced evaporation in crossed beam optical traps, to study strategies to mitigate the deleterious effects of large populations of atoms which can accumulate in the extended "wings" of the anharmonic total potential. We find that the wing region of the total potential can accumulate enough atoms so as to significantly influence the rate at which the phase space of the dimple population increases towards quantum degeneracy. Moreover, we find that by applying a relatively gentle tipping gradient to the total potential, the wings population can be suppressed, speeding up the evaporation process and greatly decreasing the sensitivity of the process to such initial conditions as atom number, temperature, and phase space density.

In our model, we utilize Monte Carlo simulation of trajectories of thermal atoms ejected from the dimple to accurately calculate the energy flow and number flow rates into the wing, to determine the energy evolution of the non-thermal wing population, and to account for the collisional back-action of the wings on the dimple population. These non-analytic rate functions, which are significantly different from what might be arrived at through simple energetics arguments, are not simply next-to-leading order corrections, but are fundamental to the realism of our model.

Unfortunately, circumstances did not permit the comparison of our quantitative predictions to data from our own experiment. However, our multipartite model of evaporation is very general, and can be straightforwardly applied to a wide variety of trap geometries, so that we optimistically look forward to tests by others in the future.

V. ACKNOWLEDGMENTS

The authors would like to acknowledge K. Nakagawa and G. Birkl for helpful communications on the details of their experiments, and W. Dennis for advice and assistance in revising early versions of this work.

This material is based upon work supported by the U. S. Army Research Office under grant number W911NF-09-1-0179.

[1] W. Ketterle and N. J. Van Druten, Advances In Atomic, Molecular, and Optical Physics **37**, 181–236 (1996).

[2] K. B. Davis, M. O. Mewes, and W. Ketterle, Applied Physics B **60**, 155–159 (1995).

[3] O. J. Luiten, M. W. Reynolds, and J. T. M. Walraven, Physical Review A **53**, 381–389 (1996).

[4] C. S. Adams, H. J. Lee, N. Davidson, M. Kasevich, and S. Chu, Physical Review Letters **74**, 3577–3580 (1995).

[5] R. Grimm, M. Weidemuller, and Y. Ovchinnikov, Advances in Atomic, Molecular and Optical Physics **42**, 95 (2000).

[6] K. Arnold and M. Barrett, Optics Communications **284**, 3288 (2011).

[7] T. Kinoshita, T. Wenger, and D. S. Weiss, Phys. Rev. A **71**, 011602 (2005).

[8] Q. Beaufils, R. Chicireanu, T. Zanon, B. Laburthe-Tolra, E. Maréchal, L. Vernac, J.-C. Keller, and O. Gorceix, Phys. Rev. A **77**, 061601 (2008).

[9] J.-F. Clément, J.-P. Brantut, M. Robert-de-Saint-Vincent, R. A. Nyman, A. Aspect, T. Bourdel, and P. Bouyer, Phys. Rev. A **79**, 061406 (2009).

[10] C.-L. Hung, X. Zhang, N. Gemelke, and C. Chin, Phys. Rev. A **78**, 011604 (2008).

[11] S. Kumar, S. Hirai, Y. Suzuki, M. Kachi, M. Sadgrove, and K. Nakagawa, Journal of the Physical Society of Japan **81**, 084004 (2012).

[12] T. Lauber, J. Küber, O. Wille, and G. Birkl, Phys. Rev. A **84**, 043641 (2011).

[13] D. Comparat, A. Fioretti, G. Stern, E. Dimova, B. LaburtheTolra, and P. Pillet, Phys. Rev. A **73**, 043410 (2006).

[15] We note that our use of p_{coll} differs from that of Ref. [13].

[15] We use gridMathematica to perform our numerical calculations. Our code is available upon request.

[16] Note1, we note that our use of p_{coll} differs from that of Reference [13].

[17] Note2, we use Mathematica and Mathematica lightweight grid manager. Our code is available upon request.

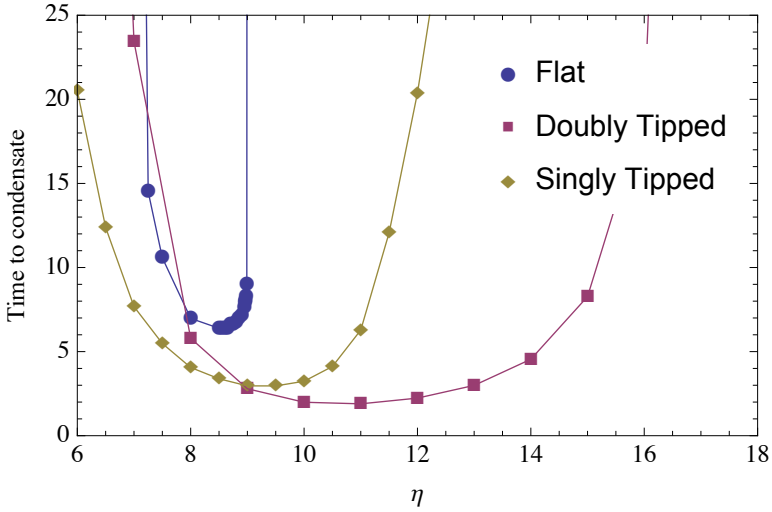

FIG. 10. (Color online) Time-to-condensation t_c for flat traps (blue circles), singly tipped traps (gold squares), and doubly tipped traps (red triangles). In these calculations, there is no loss term due to background gas collisions.

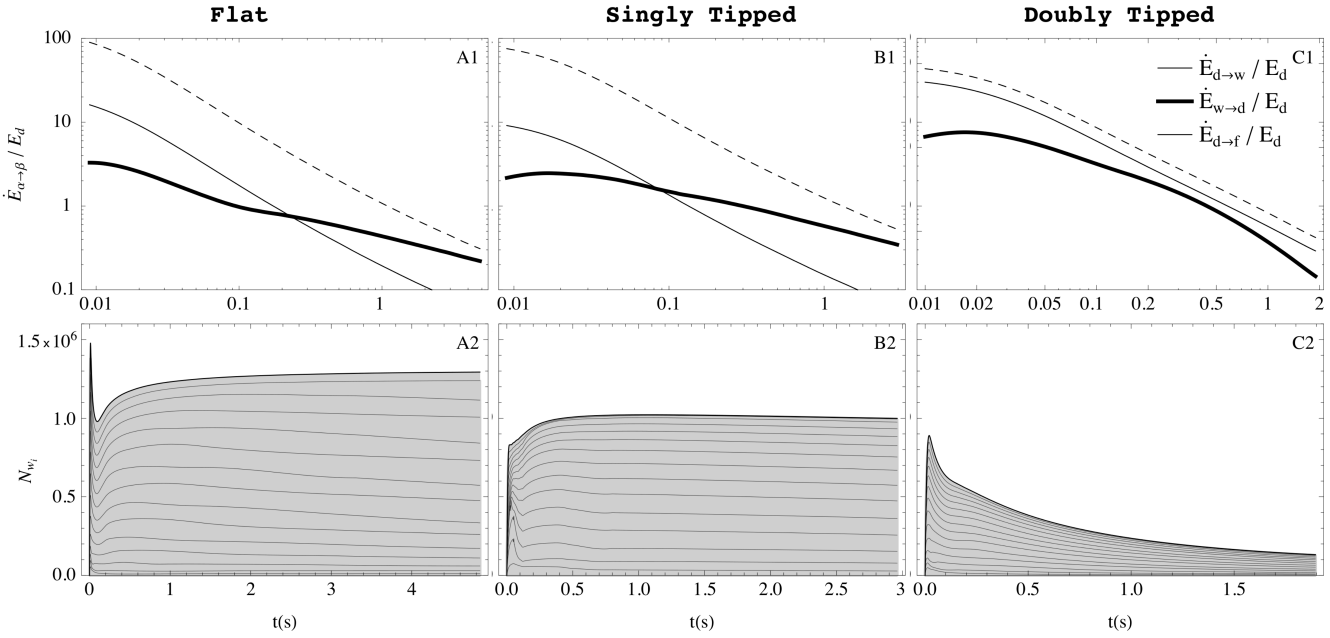

FIG. 11. Evaporation calculations for the flat trap (A1,A2), singly tipped trap (B1,B2) and doubly tipped trap (C1,C2). Top row: Rates of energy flow scaled by the total trap energy in the dimple $\dot{E}_{d\to w}/E_d$ (Blue),$\dot{E}_{d\to f}/E_d$ (Gold), and $\dot{E}_{w\to d}/E_d$ (Red). Bottom row: stacked area plots representing the wing population versus time. Each shaded band in the stack represents the population in one wing bin, from i=1 at (bottom band) to i=15 (top band). Note how the wings populations in the flat and singly tipped traps reach (quasi-) steady states, whereas only in the doubly tipped case is the wings population steadily depleted as the dimple evaporation progresses towards condensation.

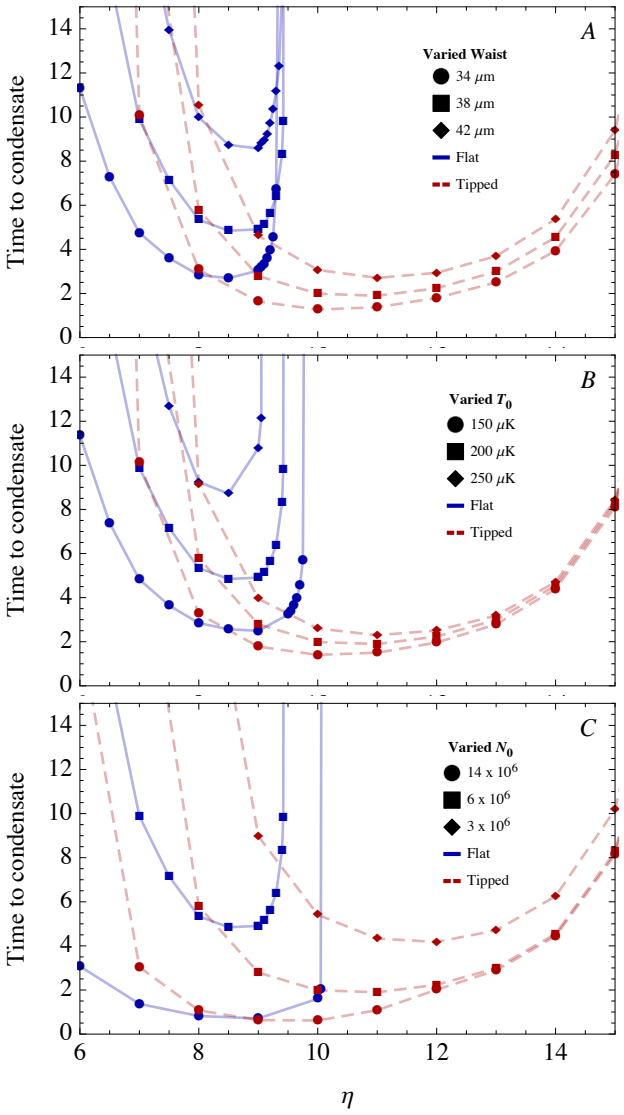

FIG. 12. (Color online) Time-to-condensation t_c versus η for evaporation in a flat (blue points) and doubly-tipped (red points) traps, for various choices of beam waist (A), initial temperature (B), and initial number (C). The lines are guides to the eye. Note that in panel (C) there are no points associated with the lowest number evaporating in the flat trap, as this set of conditions did not yield a condensate in 100 seconds of simulation time.

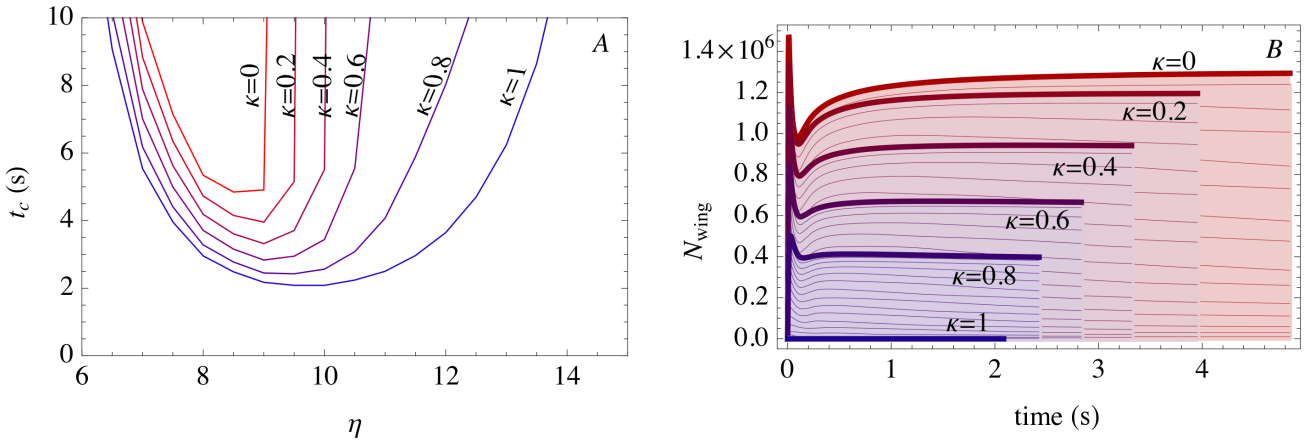

FIG. 13. (Color online) The influence of wing population revealed by adding to our physical model a fictitious, tunable loss rate for wing atoms. (A) Time-to-condensate t_c versus η for $\kappa = (0, 0.2, 0.4, 0.6, 0.8, 1)$. The red curve ($\kappa = 0$) is identical with a true flat trap. The green curve is a trap with the same physical (i.e. flat) potential, but with the wing population eliminated by setting $\kappa = 1$. The effect of a large wing population to degrade efficient dimple evaporation is revealed in the contraction of the range of viable η's for larger the steady-state wing populations. (B) Time evolution of the wing population, at optimal values of η, for the same choices of κ as in (A).